RESEARCH



The effect of synthesis parameters on the adsorption capacity of Cu⁺² ions of mullite containing polymer composites

Salar Moradi¹ · Sahar Mollazadeh Beidokhti¹ · Jalil Vahdati Khaki¹ · Morteza S. Hosseini¹ · Alireza Kiani Rashid¹

Received: 8 June 2024 / Revised: 26 October 2024 / Accepted: 13 November 2024 © Australian Ceramic Society 2024

Abstract

This study aims to synthesize mullite powders using the sol-gel method and explore their potential for water purification and removing copper ion contaminants. The effects of synthesis temperature, pH value, and solvent type on the samples' specific surface area and microstructural properties were thoroughly examined. The impact of different solvents, including aqueous and aqueous-polymeric solvents, was also investigated. Subsequently, the adsorption properties of the PVA membranes containing synthesized materials as adsorbents in a solution containing copper ions were investigated. According to XRD results, samples treated under acidic conditions in the presence of polyethylene glycol as solvent demonstrated crystallization of 100% of the mullite phase at lower temperatures (1350 °C) which is higher than that of samples synthesized at basic conditions or in aquas media. BET results and SEM images of the thermally treated samples at 1350 and 1550 °C revealed that the acid-treated samples, PW0 and W0, exhibited more porous and uneven surfaces than the basic-treated samples, PW13 and W13. According to BET and PSA results, synthesized samples at acidic conditions in a polymeric substrate demonstrated a higher specific surface area (11 m³/g) and smaller particle size (0.4 μ m) in comparison to samples synthesized in the basic and/or aqueous substrate conditions. These characteristics enhance the adsorption capacity of the synthesized materials in this series. Moreover, ICP results indicated that the PW0-1550–1 h sample exhibited the highest adsorption capacity. Under the conditions using 0.06 g of this adsorbent, the adsorption rate was 58%, and increasing the adsorbent amount to 0.12 g resulted in a 70% adsorption rate.

 $\textbf{Keywords} \ \ Mullite \cdot Sol\text{-}gel \cdot Adsorption \cdot PVA \ membrane \cdot Environmental \ remediation \cdot Wastewater$

Introduction

While some heavy metals are essential for human health in minimal amounts, they act as toxic materials at higher concentrations. The uncontrolled discharge of heavy metals into wastewater is one of the ways that can lead to the undemand increase in the concentration of mentioned ions and cause environmental damage by accumulating toxic substances in living organisms [1, 2]. Such as many other heavy elements, copper has a dual effect on both human health and environmental protection. In controlled values, it is an essential element for the progress and completion of some important biological and industrial processes. However,

excessive amounts of Cu can contaminate soil and water sources, impacting plant growth and threatening the health of living organisms. Accordingly, responsible management and proper disposal of copper waste are essential to minimize its harmful effects [2, 3]. In recent years, various methods have been proposed for removing heavy metals from wastewater, including chemical precipitation, adsorption, ion exchange, membrane filtration, and electrochemical techniques [4–6]. Among these methods, adsorption has been extensively studied due to its high removal efficiency, significant capacity, and simplicity. Numerous adsorbents have been developed for heavy metal removal from water [7–9]. Nonetheless, some limitations, such as low specific surface area and poor adsorption performance, restrict the application of these adsorbents in wastewater treatment [10].

Among different materials, porous ceramics have gained popularity as adsorbents in applications such as wastewater filtration, catalyst support, and membranes, owing to their advantageous chemical inertness [11]. Published

Published online: 02 December 2024



Sahar Mollazadeh Beidokhti mollazadeh.b@um.ac.ir

Department of Materials Engineering, Faculty of Engineering, Ferdowsi University of Mashhad (FUM), Azadi Sq, Mashhad, Iran

results indicate that aluminium oxide, aluminium hydroxide, and aluminium oxyhydroxide have been extensively studied due to their excellent physicochemical properties for Cr (VI) removal. Besides, mullite, an aluminosilicate based ceramic renowned for its exceptional physiochemical properties and high-efficiency production methods, can be used effectively as an adsorbent [1]. The significant specific surface area, porous structure, fine particle size, and electrochemical activity, making mullite particle suitable for the adsorption and removing of heavy elements [12]. According to the studies conducted by Treto-Suárez et al., aluminosilicate hydrate was utilized for heavy metal removal from wastewater [1]. Zhang et al. also demonstrated that mullite/wisconsinite porous ceramics can be prepared and modified to absorb and remove copper ions from wastewater [2]. Based on the published results by Omer Fouad et al., mullite nano-ceramic materials synthesized via the sol-gel method could be used as selective electrodes to estimate the levels of carcinogenic ion Cd(II) in biological samples [13]. Cuo et al. prepared a mullite fiber ceramic membrane coated with alumina for gas purification, achieving 100% adsorption efficiency for suspended particles ranging from 3 to 10 micrometers [14]. Since making porous ceramic bodies is a complicated and costly process, ceramic adsorbents are usually used in granular or powder form. However, the powder-based adsorbents also present drawbacks, such as the agglomeration of fine particles and costly recovery equipment [15]. Besides, when using the adsorbent in powder form, after adsorption, it is necessary to employ filter paper or centrifugation for separation processes, which is time-consuming and adds extra costs to the process [16]. Polymeric membrane-based adsorbents could be considered suitable options to overcome this issue. Due to the inherent properties, such as desired mechanical properties and the flexibility to be processed into different modules, the membrane used in water and wastewater treatment allows specific components to pass through more rapidly than others [17, 18]. Since, one important drawback of using membranes is their susceptibility to fouling and pore-clogging, modifying membranes structure by employing composite structures is one practical method in improving their antifouling properties [19]. Composite membranes are composed of discrete and continuous phases in which ceramic particles are dispersed as the discrete adsorbent phase within the polymeric matrix (continuous phase) [20]. Among different polymers, polyvinyl alcohol (PVA) is a promising candidate to use as a polymeric matrix due to due to controllable water solubility, favorable film-forming properties, and high resistance to organic fouling. The high solubility of PVA in water can be decreased by cross-linking the surface through a crosslinking reaction followed by an appropriate annealing step [21]. Different ceramic phases could be dispersed in the polymer matrix and act as adsorbents. As mentioned earlier,

mullite is a valuable adsorption agent, and the preparation method strongly affects the purity and performance of an adsorbent [22-25]. Various methods could be used for mullite production, including melting, sintering, spray pyrolysis, hydrolysis, deposition, solution combustion, and sol-gel [26]. It can also be formed from oxides or hydroxide salts of metal compounds [27–32]. Among these methods, the sol-gel process is particularly important due to its repeatability, lower synthesis temperature, lower impurity levels, and high homogeneity [32]. In the sol-gel process, hydrolysis and condensation are crucial steps that significantly impact the properties of the resulting materials. According to published results, the rate of hydrolysis and condensation of precursor materials and the rate of SiO₂ and Al₂O₃ combination depend on various factors such as the amount of water, solvent type, catalyst, pH, and temperature [33]. Besides, using polymers as the solvents of starting precursors resulted in the formation of more uniform and purer mullite at lower temperatures [22–26, 32–34]. Anicamur et al. demonstrated that under acidic conditions, the precursor gel forms crystalline mullite at a temperature of 1250 C°, while under higher pH conditions, the primary phase is α-Al₂O₃. These findings indicate that the precursor pH can influence the gel properties, mullite formation, and microstructural characteristics [35]. Although many studies have been conducted on the synthesis of mullite particles by sol-gel method, the investigation on the synergistic effect of synthesizing parameters, i.e., pH level, solvent type, and process temperature on the final physio-chemical properties of the synthesized powders, has not been systematically addressed yet. Phase purity, particle size, and porosity, which significantly influence the final application's efficiency as an adsorbent, are some physical properties directly influenced by manipulating the synthesizing parameters. At low pH, larger particles form due to a slower rate of hydrolysis and condensation processes, in comparison to basic pH. The material may have a more disordered structure due to inhibited network growth. On the other hand, high pH levels encourage rapid hydrolysis and condensation, producing smaller, more uniform particles which could be often desired for applications requiring specific geometrical properties and specific surface areas.

Accordingly, the recent study aimed to use mullite particles synthesized by the sol-gel method as adsorbents of copper ions from aqueous media. For this purpose, the parameters effective in the synthesis process were changed simultaneously so that the mesoporous aluminosilicate particles with the highest weight% of the mullite phase, the best morphology, and specific surface area were synthesized. Compared to other studies, the principal advantage and significance of the current research is to evaluate the parameters that affect the formation of mullite with an appropriate specific surface area and morphology, thereby facilitating the achievement of maximum adsorption capacity. Since



separating mullite particles from wastewater containing copper ions, after the process of ion adsorption, is time-consuming, PVA composite membranes containing synthesized mullite particles as adsorbents were used for water treatment. To the best of our knowledge, mullite-PVA composite membranes have never been used for the water treatment process.

Experimental

Alumino-silicate particle synthesis process

Tetraethyl orthosilicate (TEOS, Merck) and aluminium nitrate nonahydrate (Merck) were utilized as the silica and alumina sources, respectively, while ethanol, polyethylene glycol (PEG), and distilled water were employed as solvents [12, 36, 37]. Nitric acid (Merck) and ammonium hydroxide (Merck) were utilized as catalysts, as well [38, 39]. The required raw materials and their corresponding quantities for each experimental set are detailed in Table 1.

Four experiments employed the sol-gel method to synthesize mullite particles. The initial solution was formulated by dissolving the desired amount of aluminium nitrate in water [39, 40]. Distilled water and ethanol were mixed via a magnetic stirrer for 20 min to prepare the silica solution. Subsequently, specific amount of TEOS was meticulously added dropwise to distilled water and ethanol solution over 20 min at 60 °C to initiate hydrolysis [41]. Besides, 2 mL of polyethylene glycol with a molecular weight of 6000 g/mol was added to the initial TEOS sol as a polymeric solvent. The influence of the pH and the polymeric solvent was examined in the first and second experiments. The pH level was consistently maintained following the addition of the catalyst. An acidic environment was established at a pH of 0 (first experiment) using nitric acid, while a basic environment was achieved with a pH of 13 (second experiment) using ammonium hydroxide. The pH remained constant throughout the entire procedure. The mixtures were stirred within the sealed glass vessels, ensuring isolation from contact with air. Following the introduction of the initial aluminum

Table 1 Raw materials and their respective quantities for each experiment

Raw Material	Quantity
Ethanol	20 ml
Water	13 ml
Aluminium nitrate nonahydrate	10 g
TEOS	2 ml
polyethylene glycol (PEG)	0.6 g for each membrane

nitrate solution to the silica sol, stirring ensued under the same conditions at a temperature of 60 °C until the sol transformed into a gel. The resulting gel was aged for ten days. Subsequently, the gels were subjected to a drying period of 24 h to eliminate excess liquids and obtain xerogels. The third and fourth experiments followed the same protocol as the first two, except in these series of experiments, only one aqueous solvent was used, and the polymeric solvent was not added. The resultant samples were systematically labeled with abbreviations, as shown in Table 2.

To induce the crystallization of the mullite phase in all samples and investigate the influence of temperature, the dried gels were subjected to heating at a rate of 5 °C/min. Initially, they were elevated to a temperature of 400 °C and maintained at this temperature for 3 h. Then, employing the same heating rate, they attained temperatures of 900, 1100, 1250, 1350, and 1550 °C, undergoing thermal treatment for an additional 3 h. Finally, the obtained powder samples were cooled in a turned-off furnace.

Composite and polymer membrane preparation

6 gr of polyvinyl alcohol (PVA) were combined with 6 mL of water at a temperature of 60 °C for 20 min using a magnetic stirrer. Subsequently, 0.06 g of powder samples, including PW13-1550, W0-1550, W13-1500, PW0-1550, PW13-1100, W0-1100, W13-1100, and PW0-1100, was introduced into the PVA solution and stirred for 10 min. Additionally, a polymer solution without the synthesized aluminosilicate powder was prepared. The resulting solutions were poured into lens-shaped containers and positioned in a freezer at -20 °C for 24 h. Following this, they were dried in a freeze-dryer for another 24 h. To cross-link the membranes, a glutaraldehyde solution was applied to the freeze-dried membranes; for this, prepared membranes were sealed in a container and suspended in the vapor of glutaraldehyde for 24 h [42]. The Adsorption test methodology was as follows:

For a Cu²⁺ ion solution formulation, 4.0 g of copper nitrate was dissolved in 1 L of deionized water. Afterward, the produced membranes, without synthesized particles and with synthesized particles, were affixed to

Table 2 Series of experiments and samples systematically labeled with abbreviations

Experiments	Sample	Label
Samples with a constant pH and	pH=0	PW0
polyethylene glycol	pH = 13	PW13
Samples with a constant pH with-	pH = 0	W0
out polyethylene glycol	pH = 13	W13



a plastic mixer and mechanically stirred at a rate of 120 RPM within the container containing 50 mL of the Cu²⁺ ion solution. Sampling for ICP testing was performed at 15, 30, and 60-min intervals, with each sample having an equal amount of 10 mL. The respective sample codes are outlined in Table 3.

Characterization

The DSA-TGA test was carried out by SETSYS Evolution-1750 With a heating rate of 10 °C/min in the normal atmosphere to determine the thermal stability and phase transition temperatures of the samples. X-ray diffraction (XRD) analysis was conducted utilizing a PHILIPS PW1730 device equipped with a Cu LFF Tube ($\lambda = 1.540598 \text{ Å}$) within the range of 10–80°. This analysis aimed to ascertain the final phase composition of the synthesized powders. The ICP test was employed to assess the quantity of copper ion adsorption by produced membranes (ICP-OES, SPECTRO ARCOS-76004555-Germany). The Brunauer-Emmett-Teller (BET) test was employed to quantify the specific surface area. Dynamic light scattering (DLS, Cordnouan Technology) analysis was used to measure the particle size distribution of the synthesized particles. Chemical bond determination was carried out using the fourier transform infrared spectrometer (FTIR), specifically the Thermo Nicolet model AVATAR 370 FT-IR (USA). The morphological examination of synthesized mullite particles following the thermal process was conducted utilizing a scanning electron microscope (SEM) (VP1450 LEO-Germany).

Results and discussion

Aluminosilicate (AIS) powders

DSC-TG

Differential scanning calorimetry (DSC) and thermogravimetric (TG) analyses were conducted on the samples, and their thermal analysis curves are depicted in Fig. 1. The TG curve reveals that all samples underwent weight loss, attributable to the reduction in water content and decomposition of volatile materials [43, 44]. This weight loss predominantly occurred between 400 and 600 °C and resulted in a 60% weight reduction. Subsequent weight loss beyond 600 °C up to 1300 °C is marginal and can be ascribed to the elimination of residual nitrates [45].

In Fig. 1a and b, corresponding to samples PW0 and PW13, the DSC curve displays exothermic peaks at temperatures of 157 and 245 °C. These peaks can be attributed to the combustion of the polyethylene glycol as the polymeric solvent (PEG) present in this series of samples [46]. Additionally, the combustion of acidic and basic functional groups and the remaining nitrates may contribute to the observed exothermic peaks. In the DSC plot of sample PW0, a partial exothermic peak is discernible at 400 °C. During the thermal treatment of the dried gel, regions enriched in alumina and silica are formed, providing nucleation sites for the heterogeneous nucleation of mullite. This phenomenon could account for the observed exothermic peak in the temperature range of 400 °C [47]. Moreover, at 1095 °C, a partial exothermic peak is evident in PW0, likely stemming

Table 3 Sample codes for ICP Analysis

Adsorbent	Time	Code	Adsorbent	Time	Code	
Feed solution	-	Feed solution	Without alumino-	15 min	Without AlS-15 M	
			silicate (AlS)	30 min	Without AlS-30 M	
				60 min	Without AlS-1 H	
PW0-1100	15 min	PW0-1100-15 M	PW0-1550	15 min	PW0-1550-15 M	
	30 min	PW0-1100-30 M		30 min	PW0-1550-30 M	
	60 min	PW0-1100-1 H		60 min	PW0-1550-1 H	
PW13-1100	15 min	PW13-1100-15 M	PW13-1550	15 min	PW13-1550-15 M	
	30 min	PW13-1100-30 M		30 min	PW13-1550-30 M	
	60 min	PW13-1100-1 H		60 min	PW13-1550-1 H	
W0-1100	15 min	W0-1100-15 M	W0-1550	15 min	W0-1550-15 M	
	30 min	W0-1100-30 M		30 min	W0-1550-30 M	
	60 min	W0-1100-1 H		60 min	W0-1550-1 H	
W13-1100	15 min	W13-1100-15 M	W13-1550	15 min	W13-1550-15 M	
	30 min	W13-1100-30 M		30 min	W13-1550-30 M	
	60 min	W13-1100-1 H		60 min	W13-1550-1 H	



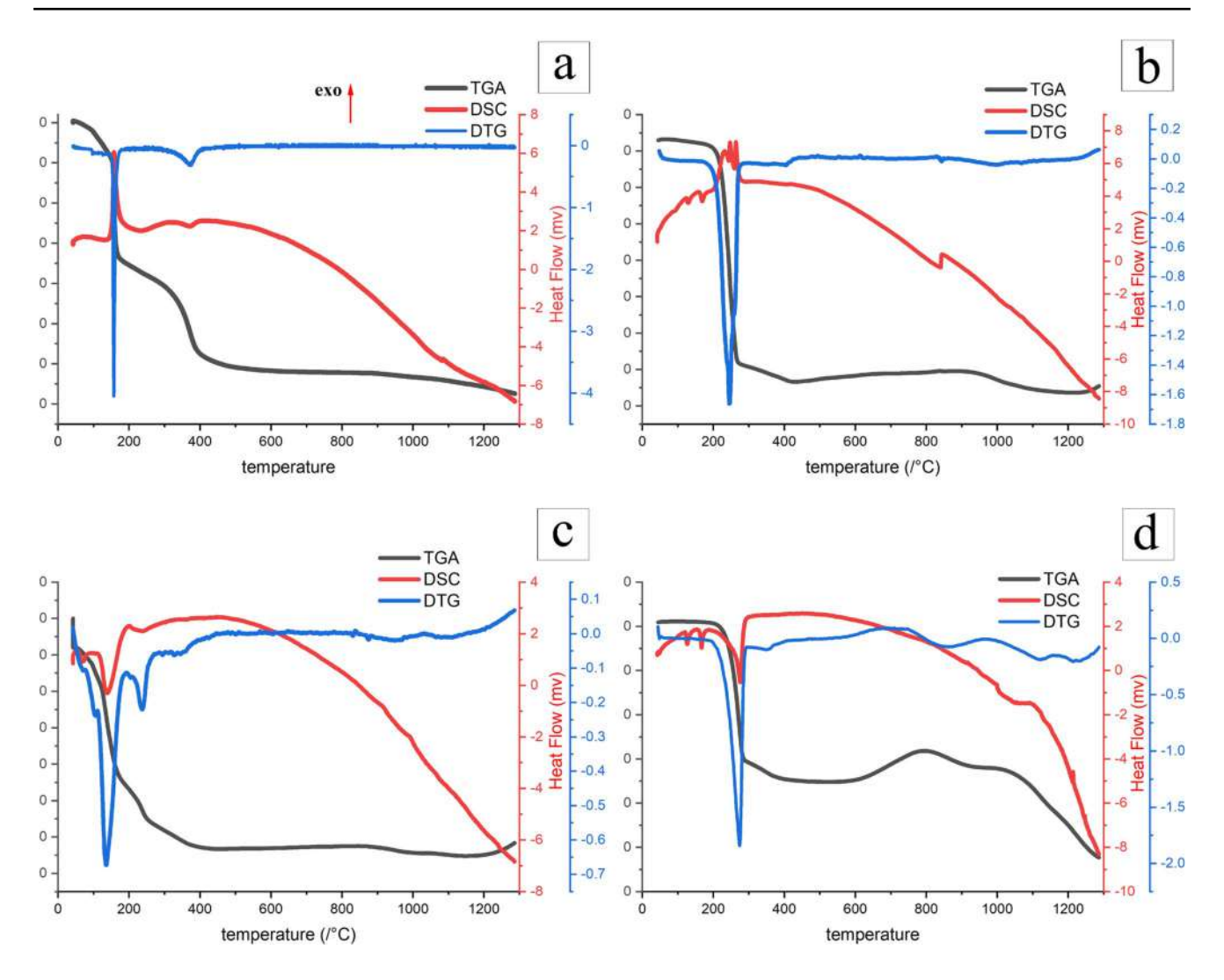


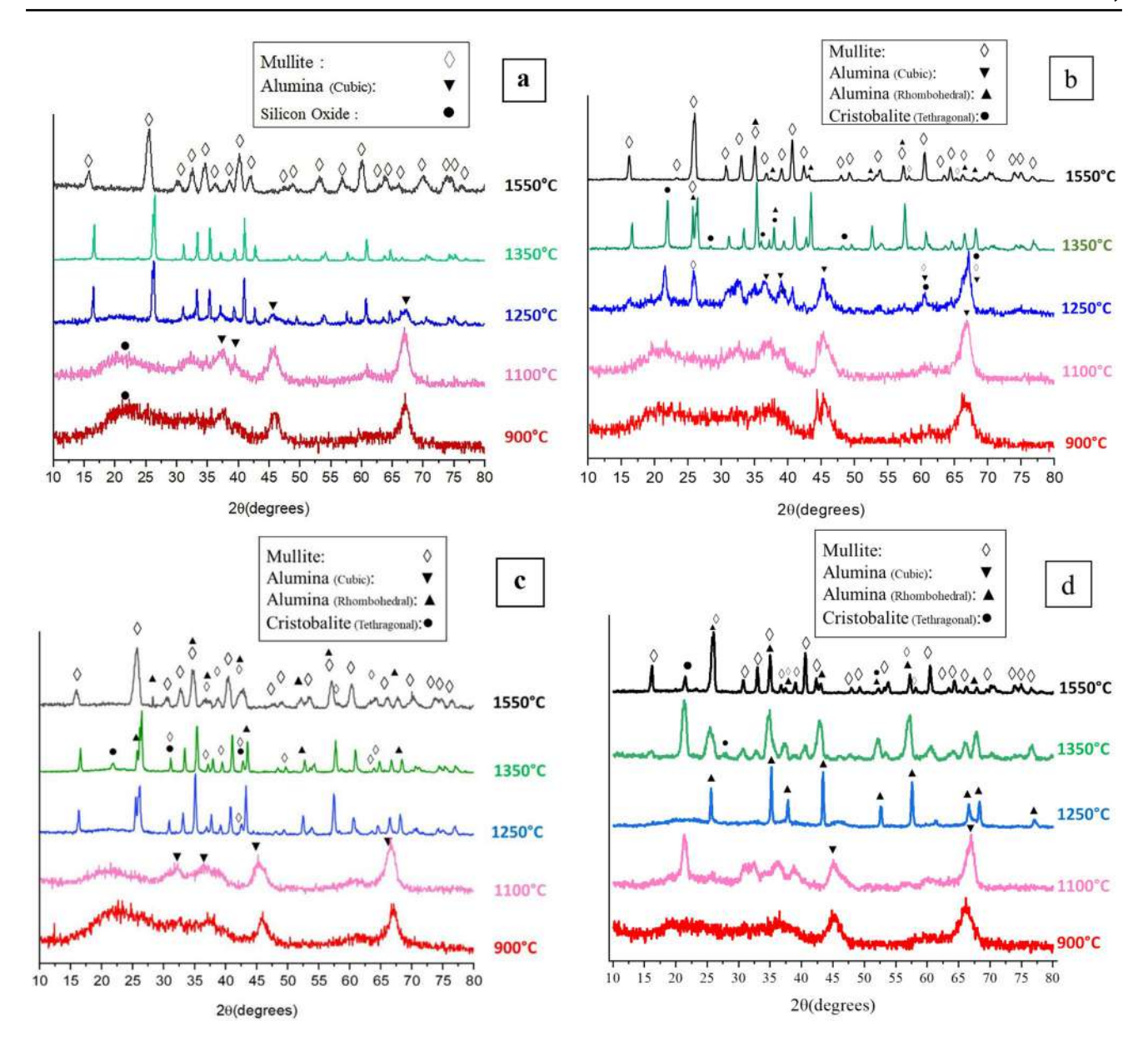
Fig. 1 The DSC-TG-DTG results for the samples (a) PW0, (b) PW13, (c) W0, and (d) W13

from the partial reactions between γ -alumina and SiO₂ [48]. This observation is substantiated by Fig. 2a and will be discussed further in the XRD results related to sample PW0. This variant of mullite exists in the form of tetragonal mullite and contains elevated levels of γ -alumina, diminishing with increasing temperature as it approaches its stable and stoichiometric composition. In sample PW13, a relatively sharp exothermic peak is revealed at 891 °C, associated with the crystallization of γ -alumina, as supported by previous literature and XRD results [48]. Furthermore, the DSC curve of sample W0 reveals exothermic peaks at 139 °C, while sample W13 exhibits exothermic peaks at 126, 167, and 275 °C, corresponding to the removal of water and volatile materials [43]. In sample W0, a small exothermic peak indicative of γ-alumina crystallization is observed at 990 °C, a finding that XRD results will corroborate. In sample W13, the 1100 °C to 1210 °C temperature range exhibits a flat region on the DSC curve and a single exothermic peak. Drawing from prior results and considering the XRD outcomes discussed below, this temperature range is attributed to the crystallization of α - and γ -alumina. Furthermore, the TG curve of W13 exhibits an abnormal weight loss of 110%, likely attributed to either the decomposition of the entire sample during the analysis process or the expulsion of the sample from the crucible due to intense exothermic reactions. The initiation of mullite crystallization was observed at 1095 °C, as indicated by the DSC curve of sample PW0. Consequently, based on these findings, the optimal temperature range for the thermal treatment of the samples is estimated to be between 1100 °C and 1550 °C.

XRD

Figure 2a and b illustrate the X-ray diffraction patterns of the synthesized samples in the presence of acidic and basic catalysts at pH values of 0 and 13 in the presence of different





 $\textbf{Fig. 2} \quad \text{XRD patterns of the synthesized samples: } \textbf{a} \text{ PW0, } \textbf{b} \text{ PW13, } \textbf{c} \text{ W0, and } \textbf{d} \text{ W13 at different heat treatment temperatures}$

aqueous-polymeric solvents heat-treated at various temperatures, respectively. In Fig. 2a, as the temperature increases from 900 to 1550 °C, the amorphous phase diminishes, and peaks associated with mullite formation become apparent, signifying the initiation and growth of the mullite phase. The absence of mullite formation in samples with a constant pH between 900 and 1250 °C can be attributed to the relatively low temperature and insufficient time for alumina to infiltrate the silica matrix. Lowering the pH and intensifying the system's acidity Increased the rate of hydrolysis and decreased the rate of condensation reactions [49]. According to Table 4a, the average crystallite size of mullite for PW0 at 1250 °C was approximately 400 Å. At 1350 °C and 1550 °C, a uniform and regular pattern accompanied by sharp

mullite peaks is observed as a result of mullite formation. According to Table 4a, with an elevation in the heat treatment temperature from 900 °C to 1550 °C, the crystallization percentage of the formed phases also experiences an increase. Ultimately, at 1550 °C, a predominantly crystalline mullite phase emerges with a crystallinity percentage of 93% (ICDD Card No. 01–073–1389). Figure 2b corresponds to samples PW13, synthesized in a basic environment with pH=13 in the presence of an aqueous-polymeric solvent and heat-treated at various temperatures. According to this figure, due to the rapid hydrolysis of TEOS compared to the hydrolysis of aluminium nitrate, there is insufficient time for significant interaction and reaction between them [50]. Consequently, the alumina phase predominantly forms during



Table 4 The quantitative results of XRD analysis for (a) PW0, (b) PW13, (c) W0, and (d) W13 samples

Sample code	T	Crystallite Size		Phase %		se %	Crystallinity %	Sample	Т	Cryst	tallite Size			Phase %	Crystallinity
code	(°C)	phase (h	kl) size	SiO ₂	Mullite	Al ₂ O ₃		code	(°C)	phase	(hkl) si	e SiC	Mullit	Al ₂ O ₃	
PW0	900	76-40	***	39		61 (gamma)	39		900		- //2	1		99 (gamma)	30
	1100	Al ₂ O ₃ (1 Al ₂ O ₃ (0 Al ₂ O ₃ (0	02) 55	25		75 (gamma)	48		1100	Al ₂ O ₃	(022) 4 (002) 5 (011) 2	0 25		75 (gamma)	52
	1250	Mullite (2 Mullite (1 Mullite (1	11) 406	3	97		66	PW13	1250	SiO ₂	(220) 2 (111) 2 (210) 9	0 12	21	67 (gamma)	65
	1350	Mullite (2 Mullite (1 Mullite (1	11) 517		100		73		1350	100000000000000000000000000000000000000	(104) 4 (113) 4 (210) 4	6 11	45	44	84
	1550	Mullite (2 Mullite (1: Mullite (3:	1) 99		100		82		1550	Mullite Mullite Mullite	(121) 2	19	93	7	83
				1	a								b		
mple	T (°C)	Crystal			Pha	se %	Crystallinity %	Sample			tallite Siz			Phase %	Crystallii
			ite Size	SiO	Pha	te Al ₂ O ₃	Crystallinity %	Sample	T (°C)	Cryst					Crystallii
		phase (ıkl) size		Pha Mull	•	Crystallinity %		207				O ₂ Mulli		Crystallin
ode	(°C)	phase () Al ₂ O ₃ (() Al ₂ O ₃ (() SiO ₂ (()	(122) 43 (102) 54 (11) 106	SiO	Pha Mull	te Al ₂ O ₃	2002		(°C)	phase SiO ₂ Al ₂ O ₃	(hkl) s	ize Si	O ₂ Mulli	e Al ₂ O ₃	30
ode	(°C)	phase (1) Al ₂ O ₃ (1) Al ₂ O ₃ (1) SiO ₂ (1) Al ₂ O ₃ (2) Al ₂ O ₃ (3) Mullite (2)	(22) 43 (02) 54 (11) 106 (04) 374 (13) 365 (10) 308	SiO 45	Pha Mull	te Al ₂ O ₃ 55 (gamma)	25		(°C) 900 1100	SiO ₂ Al ₂ O ₃ Al ₂ O ₃ Al ₂ O ₃	(111) (022) (112) (104) : (113) :	Side Side	O ₂ Mulli	99 (alpha)	30
	(°C) 900 1100	Al ₂ O ₃ ((i Al ₂ O ₃ (i) SiO ₂ ((i Al ₂ O ₃ (i) Mullite (i Mullite (i Al ₂ O ₃ (i)	(22) 43 (02) 54 (11) 106 (04) 374 (13) 365	SiO 45	Pha Mull	te Al ₂ O ₃ 55 (gamma) 95 (gamma) 44	25	code	(°C) 900 1100	SiO ₂ Al ₂ O ₃	(111) (022) (112) (104) 3 (116) 4 (111) 1 (104) 1	151 153 153 155 157	D ₂ Mulli	99 (alpha) 86 (alpha)	

the first thermal treatment stage at lower temperatures. In acidic environments, a substantial amount of alumina is dispersed in the silica matrix, whereas in basic environments, alumina is predominantly present as an oxide phase [50]. Hence, the percentage of mullite phase formed is expected to be higher in acidic environments compared to basic environments. According to Table 4b, with the heat treatment of samples synthesized in the basic aqueous-polymeric solvent environment with pH=13 and at temperatures of 900 °C and 1100 °C, two phases, γ -alumina (ICDD Card No. 01–074–2206) and SiO $_2$ (ICDD Card No. 01–076–0941), crystallize to approximately 25% and 60%, respectively. At

c

approximately 1250 °C, the mullite phase forms alongside other phases, such as γ -alumina and SiO_2 , with a crystallinity percentage of about 75%. With further increases in the heat treatment temperature, at 1350 °C and 1550 °C, the crystallinity and the mullite phase percentage increase. However, similar to the other synthesized samples, this is not a pure mullite phase and is accompanied by other phases, such as γ -alumina and SiO_2 , with a crystallinity percentage of approximately 80%.

d

Figure 2c and d depict the X-ray diffraction patterns of samples synthesized in an aqueous medium at pH = 0 and pH = 13, respectively, named W0 and W13, respectively,



and heat treated at various temperatures, as well. According to Table 4c, with the heat treatment of W0 samples at temperatures of 900 °C and 1100 °C, two phases, γ-alumina (ICDD Card No. 01-074-2206) and SiO₂ (ICDD Card No. 01–076–0941), crystallize to approximately 25% and 60%, respectively. At approximately 1250 °C, the mullite phase forms alongside other phases, such as γ -alumina and SiO₂, with a crystallinity percentage of about 75%. With a further increase in the heat treatment temperature, at 1350 °C and 1550 °C, the crystallinity and the mullite phase (ICDD Card No. 01–073–1389) percentage increase. However, the mullite phase is not pure, similar to the samples synthesized in the polymeric medium. According to Table 4d, with the heat treatment of W13 at temperatures of 1250 °C, α-alumina is observed (ICDD Card No. 01-074-0323), with crystallinity percentages of approximately 50%, and a partially crystallized mullite phase is formed. With a further increase in the heat treatment temperature, at 1350 °C and 1550 °C, the mullite phase percentage increases with the crystallinity percentages of approximately 80% and 85%, respectively.

Overall, the presence of water in the reaction system impacts the crystallization temperature of mullite and the occurrence of spinel formation. An increase in the amount of water leads to higher crystallization temperatures of mullite and an elevated likelihood of spinel formation. In polymeric media, the resulting materials tend to be more homogeneous with reduced phase separation, facilitating mullite formation at lower temperatures and in a pure form [32, 34]. According to XRD results, for the synthesized samples under both acidic and basic conditions, both in polymeric and aqueous media, the crystallinity percentage remains significantly low up to 1100 °C, and the samples can be considered almost amorphous. With an increase in the heat treatment temperature, the characteristic peaks of mullite become prominent, indicating the formation of a more stable mullite phase. The crystallinity percentage also experiences an increase with temperature due to the highly crystalline nature of the mullite phase. In general, it can be concluded that at lower temperatures, a higher percentage of the mullite phase, and, in fact, pure mullite, is obtained in samples under acidic conditions in the presence of polymeric solvent.

FTIR

FTIR analysis was employed to complement the information obtained from the XRD analysis. The chemical changes and structural bands of the synthesized samples at temperatures of 900–1100–1250–1350–1550 °C are shown in Fig. 3. The vibrations appearing around 3400 cm⁻¹ are attributed to the stretching vibration of OH in H₂O molecules [51–53]. The irregularity and complexity in the band shape may be due to the random vibrations of different energy of -OH groups [52]. Since the utilized material is Al(NO₃)₃, the gel may

contain some amounts of NO₃⁻ ions, observable by the band in the range of 1388 cm⁻¹, corresponding to the stretching of trapped NO₃⁻ ions in the gel structure [52]. Additionally, a vibration at around 1625 cm⁻¹ is attributed to the N-O functional group. The observed vibrations in the range of 1100 cm⁻¹ and 456 cm⁻¹ are attributed to asymmetric stretching and bending vibrations of Si-O-Si bonds, respectively [51, 53]. In the same vibration position at approximately 1100 cm⁻¹, it indicates the presence of a pure silica structure. Notably, the Si-O vibration in this study was observed in the range of 1180 cm⁻¹. The vibration in the range of 1100 cm⁻¹ was attributed to C-O bands. The bands at 1557 cm⁻¹ were assigned to the vibrations of Si-O-Al in the sample [53]. The vibration band at 567 cm⁻¹ was attributed to the stretching vibrations of Al-O bonds derived from AlO6 groups in mullite [51]. In the PW0 sample at a temperature of 900 °C, no band related to Al-O was observed in the range of 1570 cm⁻¹. With an increase in temperature to 1100 °C, traces of a small band in this region appeared. This band reached its maximum intensity as the temperature increased to 1350 °C and 1550 °C. Additionally, in this sample, the C-O stretching vibration appeared at around 1110 cm⁻¹ in the PW0-900 sample, with a small shoulder on its left side, most likely related to Si-O. As the temperature increased, the intensity of the C-O band gradually decreased and disappeared at 1550 °C, while the Si-O vibration band became clearly visible. Considering the XRD results obtained for the PW0-1550 sample, where mullite was received, the FTIR results with characteristic Al-O and Si-O peaks were predictable. During the heat treatment, the removal of hydroxyl groups and organic matter in the gel structure is expected. This is confirmed by the disappearance of bands related to these O-H groups in the synthesized samples with an increase in heat treatment temperature. The removal of -OH groups in the sample leads to an increase in Al-O-Al and Si-O-Si bonds. Furthermore, these two types of bonds can become more compact and result in the formation of an Al-O-Si bond [39]. It was also observed that the vibrations related to O-H were removed with increasing temperature in acidic samples. However, in basic samples, due to the basic nature of the prepared matrix and the presence of a significant amount of probable O-H groups in the system, the vibrational bands corresponding to O-H groups were still observed with increasing temperature. It should be noted that the observed O-H vibration in the acidic PW0-1550 sample could be due to the ambient moisture or the moisture of the KBr used in the analysis. After heat treatment at temperatures of 1250 °C and 1350 °C, significant spectral changes were observed in the range of 560 and 666 cm⁻¹ due to the appearance of the Al-O stretching vibration in the structure, indicating the formation of an irregular structure with multiple vibrations at low wave numbers. The vibration in the range of 1830 cm⁻¹ also became broader, indicating a



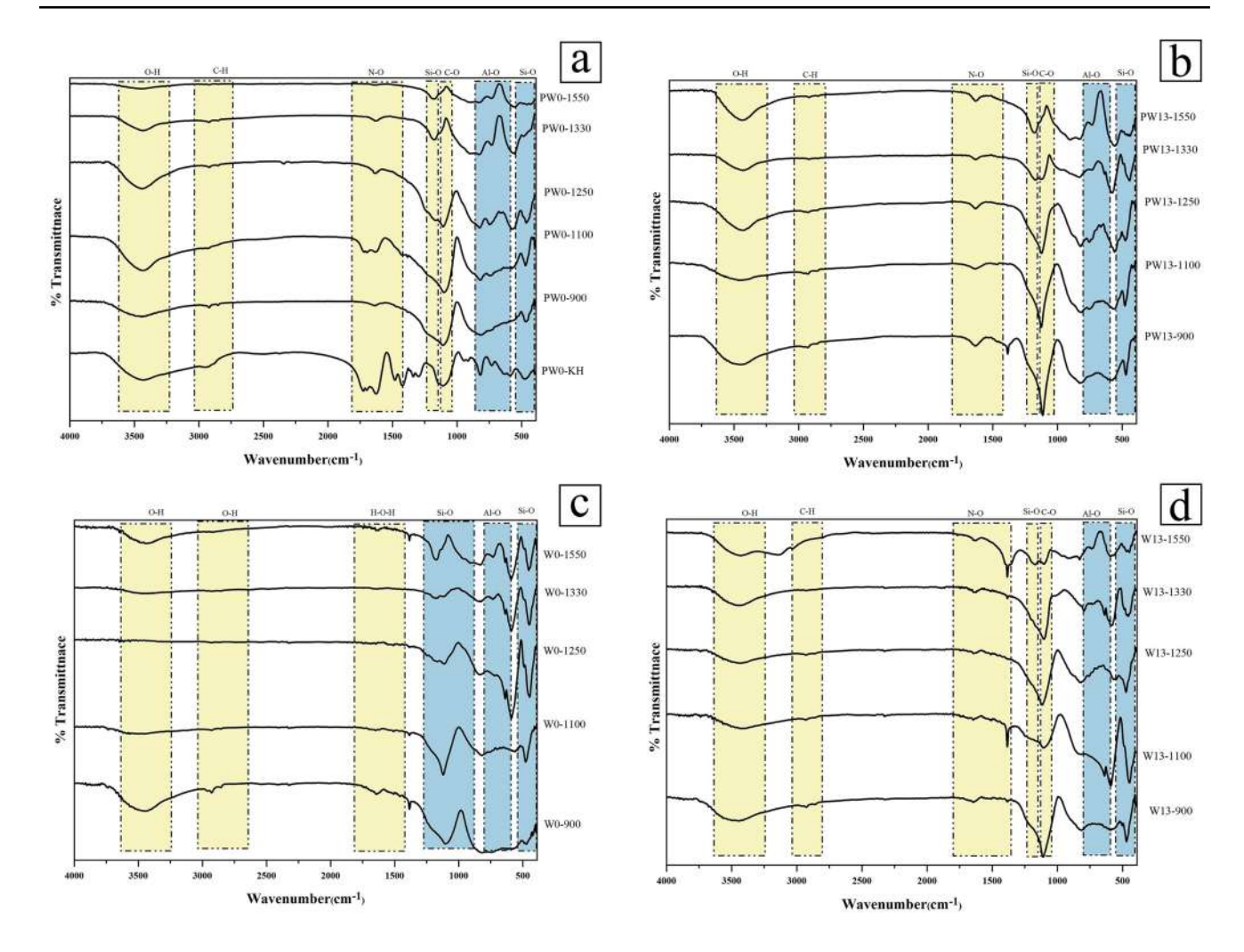


Fig. 3 FTIR spectra of samples, a PW0, b PW13, c W0, d W13

higher formation of Si-O-Al bonds, increasing the crystallization of mullite phases [52]. The observed vibration bands in the range of 1750 cm⁻¹, with the bending mode of (Si, Al)-O-(Si, Al) and a vibration band at 737 cm⁻¹, are consistent with mullite formation, as well [51].

In all samples, after heat treatment at 1550 °C, the bands present in the range of 1171 cm $^{-1}$, corresponding to Si-O-Al vibrations, became broader, indicating complete crystallization of mullite with a lower SiO_2 content. The bands in the range of 591 cm $^{-1}$ also became more prominent, indicating the presence of $\mathrm{Al}_2\mathrm{O}_3$ and $\mathrm{Al}_2\mathrm{O}_3\text{-SiO}_2$ accumulations in the structure [52]. According to the studies conducted by Sividenko and Barna [51], the assigned fundamental bands to SiO_4 (482, 988, 1107, 1131, and 1168 cm $^{-1}$), AlO_4 (620, 828, and 909 cm $^{-1}$), and AlO_6 (578 and 1482 cm $^{-1}$) demonstrate the presence or formation of mullite.

BET

Figure 4 depicts the results of nitrogen adsorption/desorption isotherms at 77 K for the heat-treated powders.

Based on the studies conducted by Brunauer, Emmett, and Teller in 1985, adsorption isotherms can be classified into six types. Comparing the graphs in Fig. 4 with this classification allows us to analyze the results. Figure 4(a) represents the adsorption/desorption isotherm of W0-900, corresponding to the hysteresis loop of type H4, suggesting the presence of slit-like and micro-void channels. Figure 4(b), corresponding to W0-1350, exhibits a type III isotherm, where the adsorbed amount increases convexly with relative pressure. This type indicates relatively weak interactions between the adsorbate and the adsorbent, and the adsorbed molecules tend to accumulate on the preferred sites of a non-porous or macro-porous



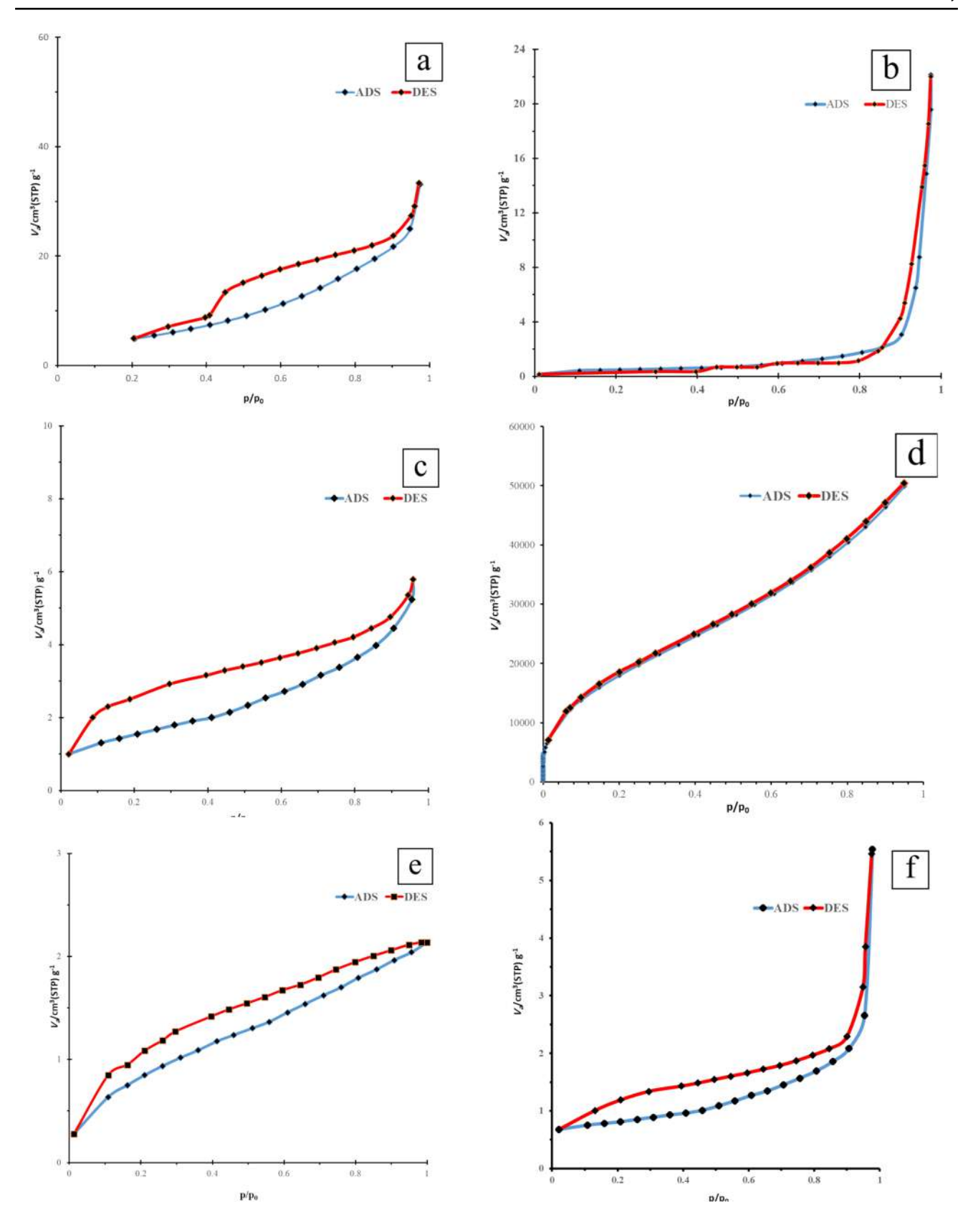


Fig. 4 Nitrogen adsorption/desorption isotherms at 77 K corresponding to the heat-treated powders:**a** W0-900, **b** W0-1350, **c** W0-1550, **d** W13-900, **e** W13-1350, **f** W13-1550, **g** PW0-900, **h** PW0-1350, **i** PW0-1550, **j** PW13-900, **k** PW13-1350, **l** PW13-1550



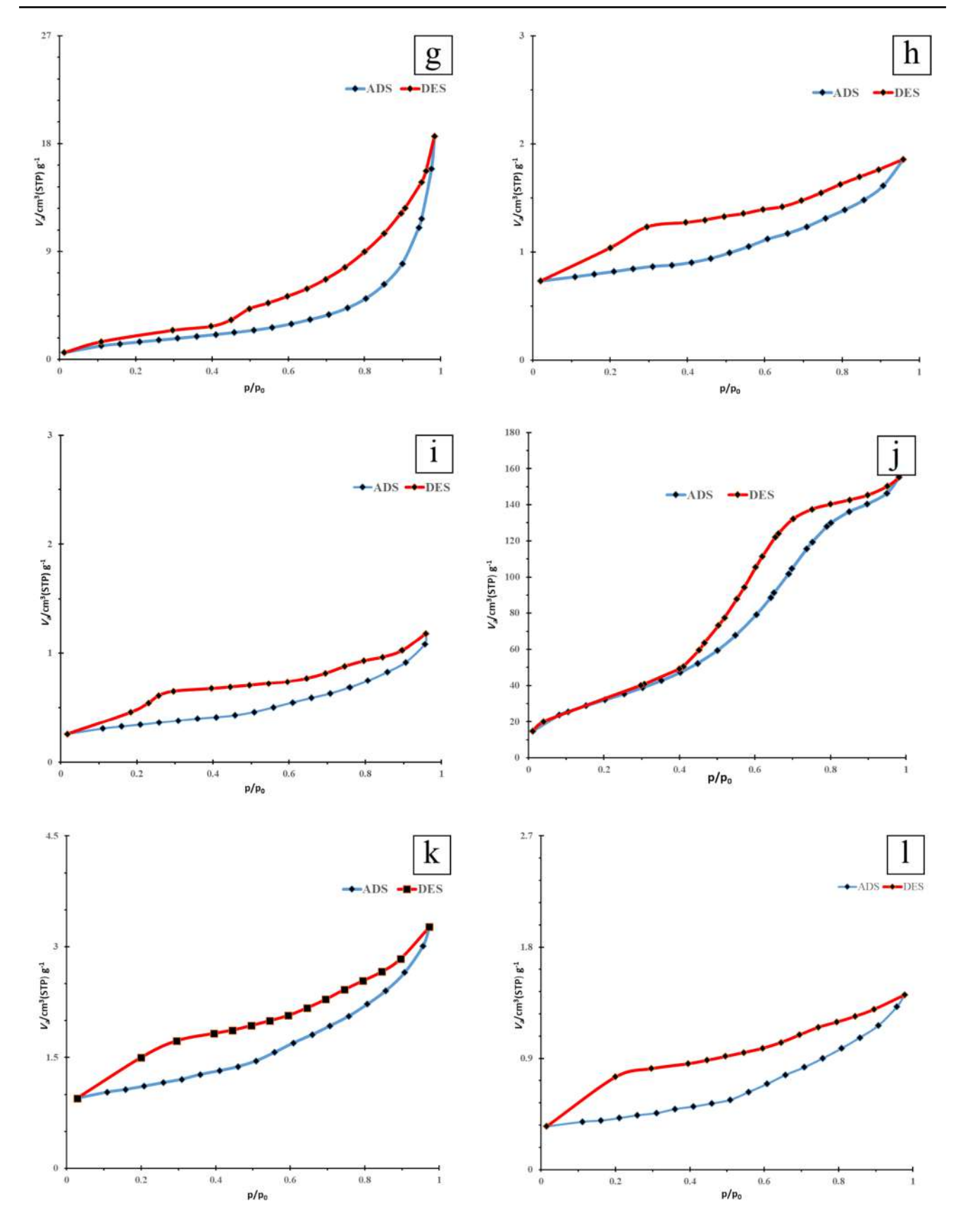


Fig. 4 (continued)

solid [54, 55]. The behavior observed in Fig. 4(c) aligns with Type IV isotherms, which are characteristic of mesoporous materials, as well. This suggests the presence of non-rigid, slit-like, and irregular-shaped pores in the corresponding sample. Figure 4(d), shows a type II isotherm. Type II is typically observed in non-porous or macro-porous materials with an unlimited number of adsorbed layers [54, 55]. The elevated specific surface area of the W13-900 sample, as documented in Table 5, can be attributed to the inherent nature of gammaalumina, characterized by a highly porous structure and substantial specific surface area [56]. The behavior observed in graphs (e)-(l) in Fig. 4 aligns with Type IV isotherms, as well, which have porous characteristics like those in Fig. 4(c) mentioned earlier. In conjunction with the BET analysis, the complementary BJH theory was employed to assess the distribution of pore sizes, particularly in materials featuring a confined range of mesopores and small macropores. The MP plot was utilized to derive the pore size distribution for pores with diameters less than 1 nm. The outcomes of the BJH and MP analyses are detailed in Table 5. The results suggest a consistent distribution of pore sizes across most samples, signifying mesoporous attributes, with pore sizes falling within the 1 to 3 nm range. PSA results are shown in Table 5, as well. According to these results, there is no significant difference between the particle sizes of different heat-treated samples at various temperatures.

SEM images

Figure 5 displays SEM images of the heat-treated samples PW0, PW13, W0, and W13 at 1550 °C. The observations reveal that the acidic sample PW0 exhibits porous and uneven surfaces characterized by many pores, indicating its potential for enhanced performance in adsorption applications.

Table 5 Results from MP and BJH theories and DLS

Sample		MP			BJH	DLS			
		$\overline{S_{BET} (m^2/g)}$	The total hole volume (cm ³ /g)	The average pore diameter (nm)	Vp (cm ³ /g)	r _{p, peak} (Area) (nm)	$(P/P_0)_h$	Particle size (µm)	
PW0	900	6	0.028758	20	0.028375	2.7	0.984	0.1	
	1350	13	0.0038865	5	0.0030687	2.1	0.990	0.5	
	1550	11	0.0031938	11	0.0029859	2.1	0.989	0.3	
PW13	900	115	0.24	8	0.2598	2.4	0.982	0.1	
	1350	14	0.0058465	6	0.0050081	2.1	0.990	0.3	
	1550	11	0.0028478	8	0.002612	2.1	0.990	0.4	
W0	900	17	0.063019	15	0.063436	1.8	0.981	0.4	
	1350	11	0.041938	108	0.037968	1.9	0.981	0.5	
	1550	15	0.017081	13	0.016378	1.8	0.983	0.6	
W13	900	11,694	82.207	28	78.397	1.2	0.990	0.1	
	1350	13	0.0032713	4	0.0031185	1.2	0.990	0.4	
	1550	12	0.012937	17	0.01204	2.1	0.982	0.2	

Adsorption results

ICP

ICP results for the filtered samples utilizing membranes without aluminosilicate powders and containing 0.6 g of the heat-treated powders at 1100 and 1550 °C as adsorbents are depicted in Figs. 6 and 7, respectively. In order to compare the effect of heat treatment temperature on the adsorption ability of synthesized powders, samples heat-treated at 1100 °C and 1550 °C were selected and used for the fabrication of composite membranes. Polymer membranes without these particles were also fabricated and used for adsorption to evaluate the effect of the presence of synthesized aluminosilicate particles on the adsorption of copper ions from the liquid medium. The control solution used to study the adsorption capability of the copper ions from water media by the fabricated composite membranes contained an initial copper concentration of 140 mg/l. According to Fig. 6, subsequent filtration using polymeric membranes devoid of aluminosilicate powders decreased the copper concentrations from 140 mg/l to 119 mg/l, 117 mg/l, and 105 mg/l for filtration durations of 15, 30, and 60 min, respectively. The absence of the aluminosilicate adsorbent in the polymeric matrix is expected to yield a low adsorption capacity of copper ions. The marginal reduction of the copper concentration in this experiment may be attributed to the presence of excellent pores in the polymeric membrane formed during the freeze-drying process. Figure 6 presents the adsorption results using membranes containing aluminosilicate particles that underwent heat treatment at 1100 °C. These membranes do not exhibit significant adsorption capacity, with the highest adsorption recorded for sample W0-1100-1 h, resulting in a copper concentration of 121 mg/l. In other words, only 13.5% of the



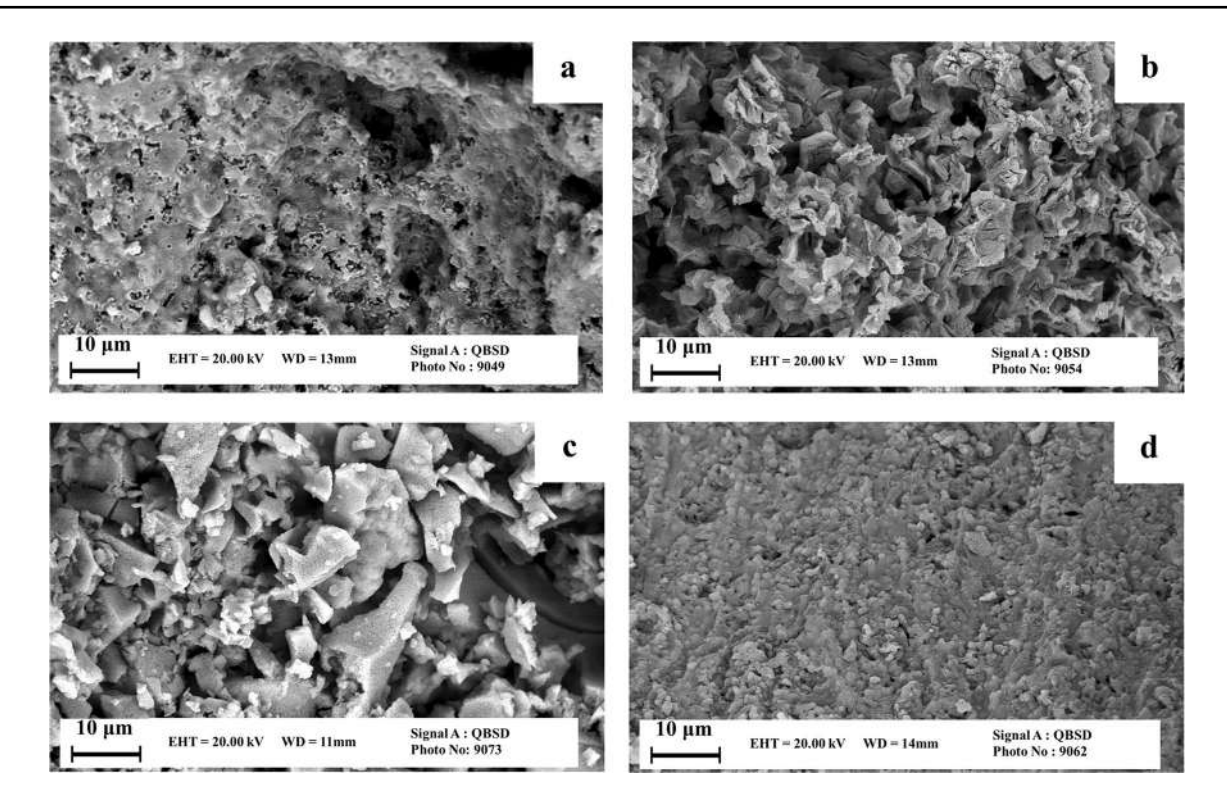


Fig. 5 SEM images of the heat-treated samples at a temperature of 1550 °C. a) PW0 b) PW13 c) W0 d) W13

Fig. 6 The ICP results for the heat-treated samples at 1100 °C with a dosage of 0.6 g of the adsorbent

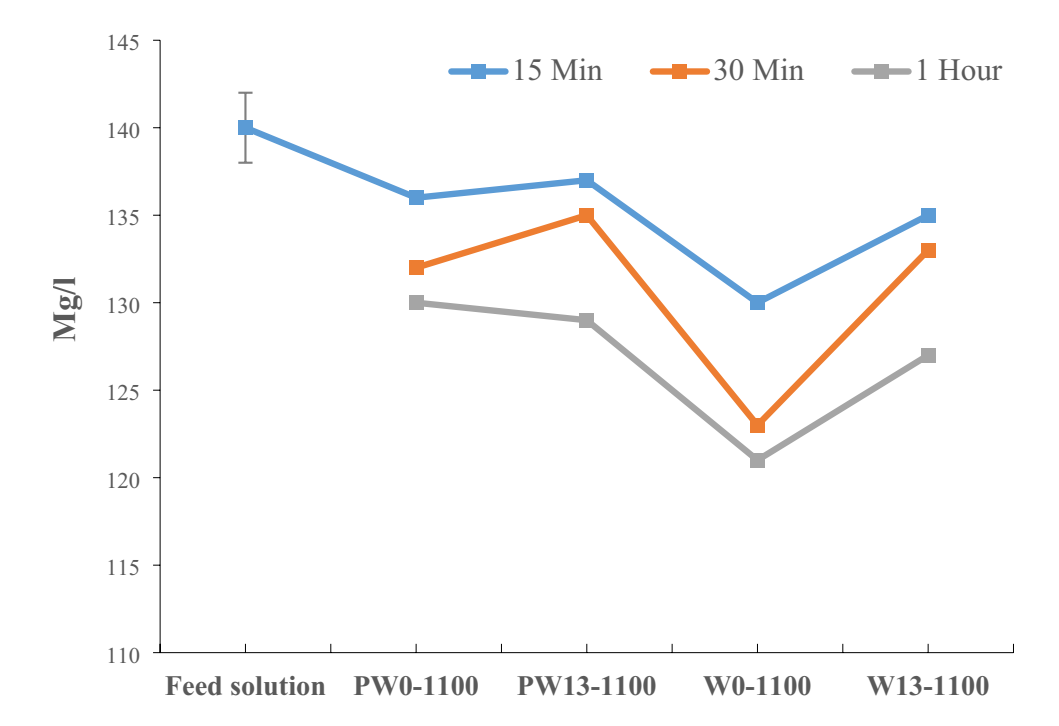
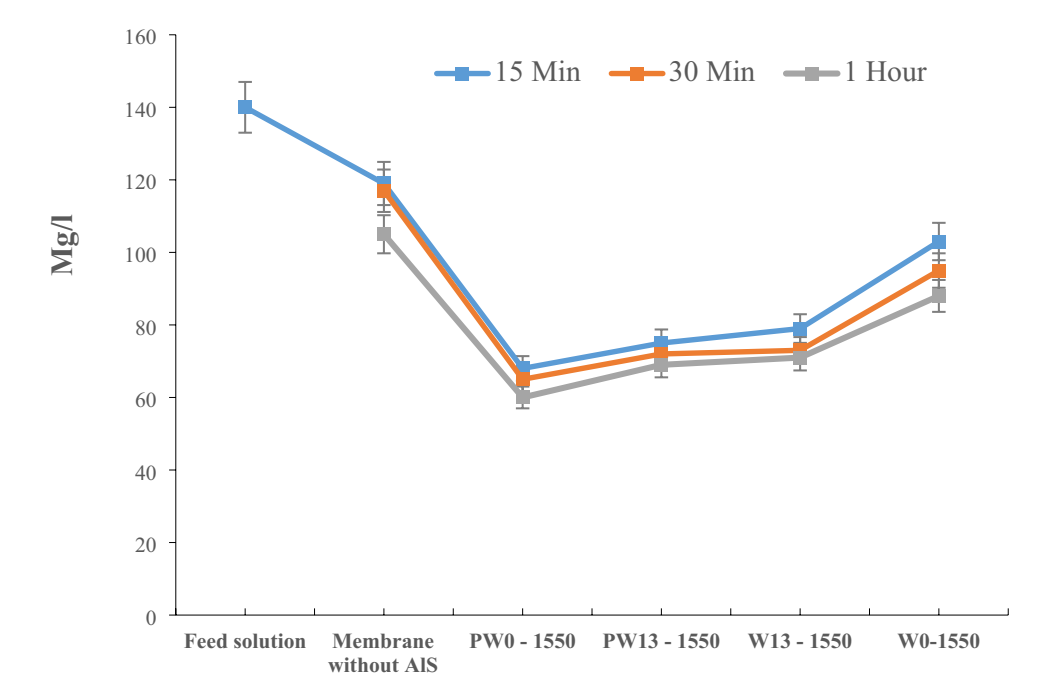




Fig. 7 The ICP results for the heat-treated samples at 1550 °C with a dosage of 0.6 g and the membrane sample without aluminosilicate



copper ions in the solution were adsorbed. These findings suggest that the membranes created using reinforcing materials heat-treated at 1100 °C are ineffective in adsorption. XRD results and Tables 1a-d indicate the absence of peaks associated with any crystalline phase in these materials.

Figure 7 illustrates the ICP results for the polymer membranes fortified with aluminosilicate particle heat treated at 1550 °C. Compared to the samples treated at 1100 °C, these samples have absorbed a higher percentage of the available copper ions from the solution, showing a significant difference in the adsorption capacity compared to the polymeric membrane without aluminosilicate particles. The highest adsorption capacity is achieved by sample PW0-1550, resulting in a copper concentration of 60 mg/l after 1 h, showing that 57% of the copper ions are adsorbed. As depicted in Fig. 4i, the adsorption isotherm of this sample resembles a Type IV isotherm associated

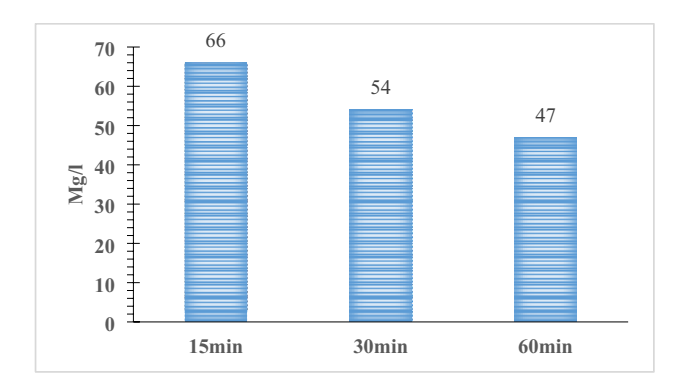


Fig. 8 The results of the ICP analysis of the adsorbed solution with a dosage of 0.12 $\rm g$

with mesoporous materials, exhibiting a hysteretic loop characteristic of non-rigid aggregates of plate-like pores [54]. These features can enhance the contact point between the adsorbent and the adsorbate, leading to a more efficient adsorption process. The experiment was extended to 60 min to ensure equilibrium conditions were reached. However, it can be observed that for all samples, after 60 min, the adsorption levels have reached a relatively constant state, and the changes in solution concentration are insignificant. Therefore, it can be concluded that the

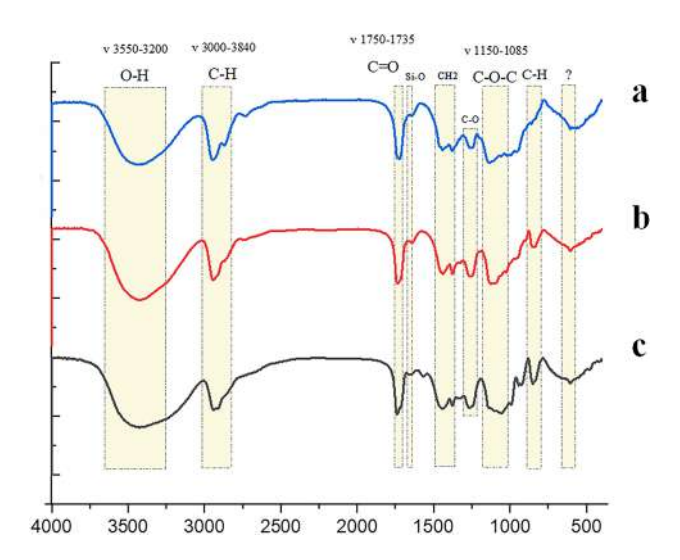


Fig. 9 The results of the FTIR test for the membrane samples:**a** The membrane containing 0.06 g of PW0-1550 before adsorption,**b** The membrane containing 0.06 g of PW0-1550 after 1 h of adsorption,**c** The membrane containing 0.12 g of PW0-1550 after 1 h of adsorption



adsorption process has reached equilibrium. The dissolution of the polymeric membrane can be considered an influential factor after 60 min. Another factor influencing the results may be the dissolution of the polymeric membrane. Despite being cross-linked with glutaraldehyde, the membrane softened upon contact with the aqueous solution, becoming gel-like. This reduced interaction between the aluminosilicate particles and the solution, potentially affecting the adsorption of copper ions.

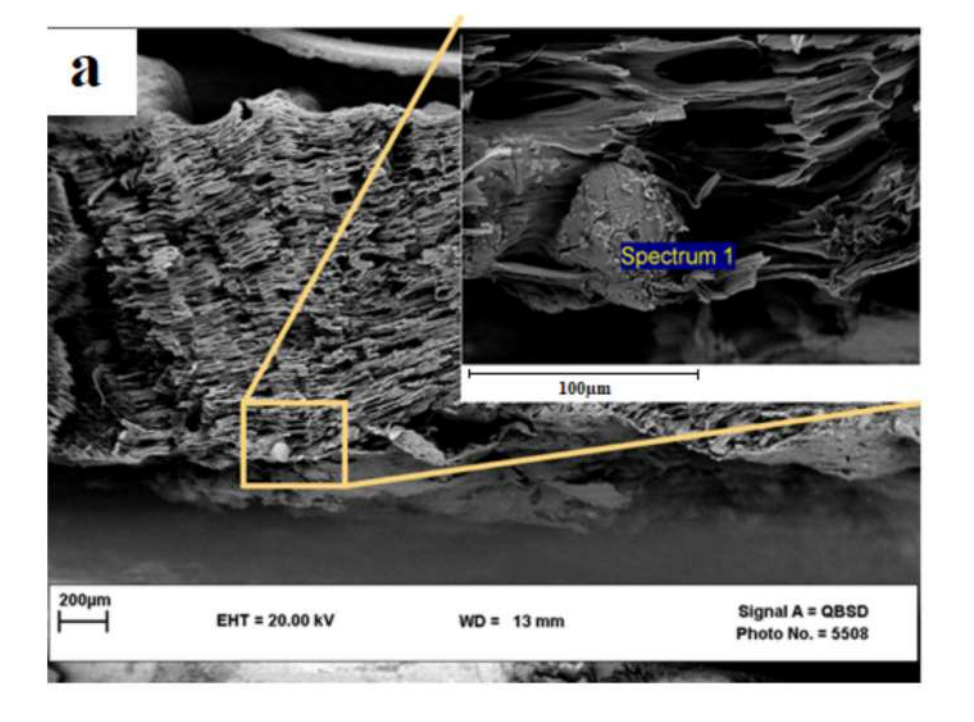
As the composite membrane containing PW0-1550 powder exhibited the highest adsorption capacity, it was selected for further experimentation with double the adsorbent dosage. A PVA membrane containing 0.12 g of PW0-1550 adsorbent powders was prepared to accomplish this.

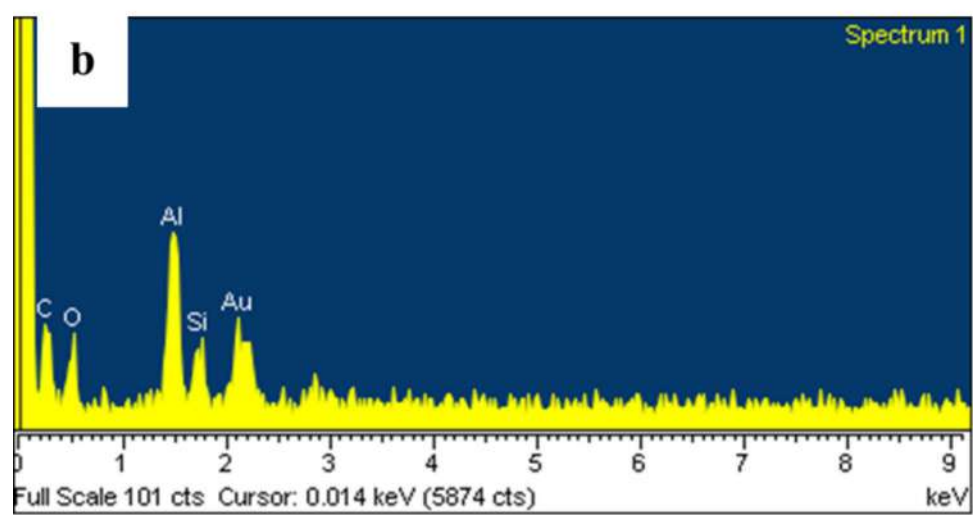
Fig. 10 a SEM images of the polymer membrane before the adsorption process. b Energy dispersive X-ray analysis (EDX) of the specified region is shown in Figure 10a

The adsorption test was repeated using the same methodology, and the results are depicted in Fig. 8. As expected, as the adsorbent dosage increased, the adsorption level during the 1-h duration rose from 58 to 70%. At the same time, the concentration of copper ions in the feed solution decreased from 140 mg/l to 47 mg/l.

FTIR results of the prepared membranes

The membranes containing PW0-1550 nanopowder with dosages of 0.06 and 0.12 g were dried after adsorption, and FTIR tests were conducted on them before and after adsorption. The results are shown in Fig. 9. According to Fig. 9, the absence of bands indicates the presence of no bonds







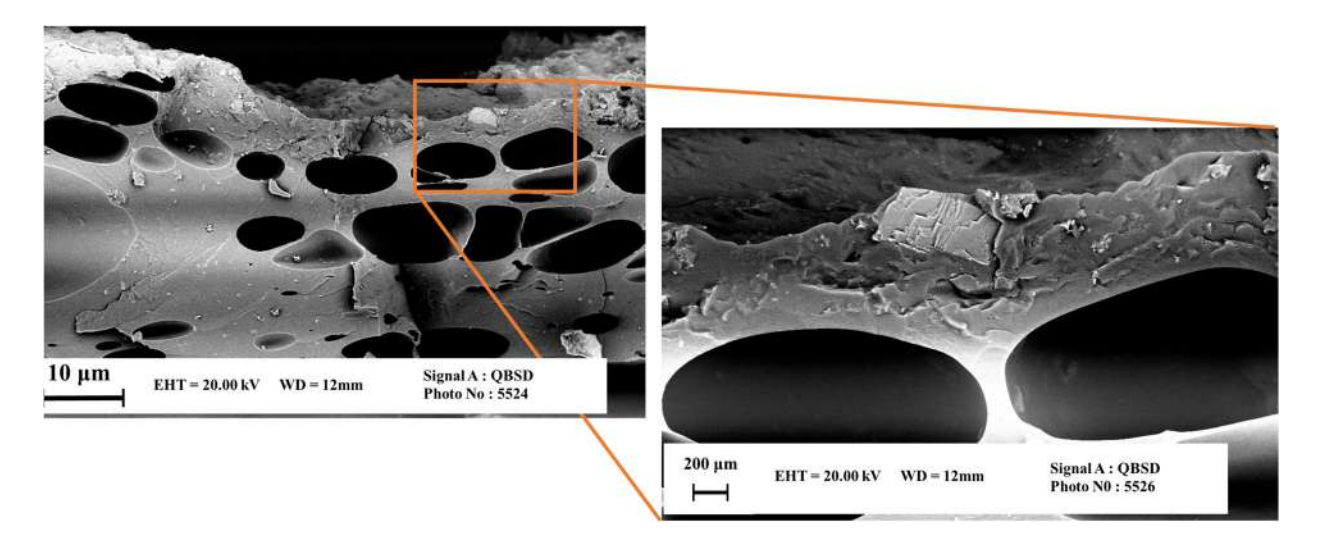


Fig. 11 SEM images of the polymer membrane after the adsorption process

between copper and the constituents of aluminosilicate particles. This suggests that the adsorption mechanism has a physical nature. The high adsorption rate and the absence of heat release or adsorption during the adsorption test align with these findings [57].

SEM images of the membranes

SEM images of the cross-sectional surface of the polymer membrane containing the PW0-1550 sample before and after the adsorption test are presented in Figs. 10 and 11, respectively. Figure 10a shows the cross-sectional surface of the polymer membrane before the adsorption process, revealing the presence of mullite particles and the porous nature of the membrane. Figure 10b displays the EDS results of the material within the membrane, indicating the presence of aluminium (Al), silicon (Si), and oxygen (O) elements, suggesting the dispersion of mullite within the membrane. The presence of carbon (C) is due to the carbonaceous nature of the PVA structure.

Figure 11 depicts SEM images of the polymer membrane after the adsorption process. The polymer membrane retains its porous nature even after adsorption and exposure to water. The porosity is visible in large cavities, and mullite particles are present in the polymer matrix, indicating that the mullite particles remain attached to the membrane and are not detached into the surrounding medium during the adsorption process.

Conclusion

The aim of the current study was to use sol-gel synthesized mullite particles as adsorbents of copper ions from containing liquid environments. Since the process of filtration and separation of adsorbent particles from the environment is a time-consuming and costly process, mullite-PVA composite membranes were fabricated by freeze-drying process and used as adsorbents. The physicochemical properties of the synthesized particles affect their ability to act as adsorbents. Since these properties are optimized by controlling the synthesis parameters, the synthesis conditions were designed so that the effect of the most significant number of variables on the properties of the final particles was studied. Accordingly, the synthesis of mullite was conducted using the sol-gel method, employing simultaneous variations of the solvent type, pH, and different heat treatment temperatures within the range of 900 °C to 1550 °C. XRD and FTIR results confirmed the successful synthesis of mullite as the predominant phase in samples PW0-1350, PW0-1550, PW13-1550, W0-1550, and W13-1550. The samples synthesized in acidic conditions in the presence of polymeric solvent displayed a notable proportion of the pure mullite phase. Besides, SEM images of the polymer membranes containing heat-treated particles revealed that the acidic samples PW0 and W0 displayed more porous and uneven surfaces when compared to the



basic samples PW13 and W13. Moreover, these samples exhibited a great specific surface area and small particle size when compared with samples prepared under basic and aqueous conditions. The ICP results demonstrated the high adsorption capacity of the PW0-1550 sample for copper ions. The polymer membrane containing 0.06 g of PW0-1550 powder demonstrated an adsorption percentage of approximately 58% for copper ions. With an increased amount of adsorbent to 0.12 g, the adsorption percentage rose to around 70%. The FTIR results of the membranes utilized in the adsorption process indicated that the adsorption mechanism was predominantly of a physical nature.

Declarations

Competing interests The authors declare that they have no known competing financial interests or personal relationships that could have appeared to influence the work reported in this paper.

References

- Treto-Suárez, M.A., et al.: Kinetic study of removal heavy metal from aqueous solution using the synthetic aluminum silicate. Sci. Rep. 10(1), 10836 (2020)
- Zhang, Y., et al.: Preparation and Modification of Mullite Whiskers/Cordierite Porous Ceramics for Cu2 + adsorption and removing. ACS Omega. 5(25), 15691–15701 (2020)
- Gupte, A., Mumper, R.J.: Elevated copper and oxidative stress in cancer cells as a target for cancer treatment. Cancer Treat. Rev. 35(1), 32–46 (2009)
- Tuas, M.A., Masduqi, A.: Treatment of copper-contained Jewellery Wastewater by Precipitation and Adsorption using Rice Husk Charcoal. J. Ecol. Eng. 20(4), 94–103 (2019)
- Li, C., et al.: Boosting the growth and aggregation of sulfide nanoparticles via regulating heterogeneous nucleation for enhanced sedimentation. Environ. Science: Nano. 10(2), 454–462 (2023)
- Ren, Y., et al.: Porous poly(ionic liquid) membranes as efficient and recyclable absorbents for heavy metal ions. Macromol. Rapid Commun. 38(14), 1700151 (2017)
- Zhao, G., et al.: Few-Layered Graphene Oxide Nanosheets as Superior Sorbents for Heavy Metal Ion Pollution Management, vol. 45, pp. 10454–10462. Environmental Science & Technology (2011). 24
- 8. Osman, N.S., Sabri, M.A.M., Sapawe, N.: Synthesis of mesoporous silica nanoparticles from Oil Palm Frond based silica to enhanced removal of Heavy Metal. Mater. Sci. Forum. **1076**, 221–227 (2022)
- Cao, C.-Y., et al.: Low-cost synthesis of Flowerlike α-Fe2O3 nanostructures for heavy metal ion removal: Adsorption property and mechanism. Langmuir. 28(9), 4573–4579 (2012)
- Sobhanardakani, S., Zandipak, R., Taghavi, L.: Synthesis of 2,4-dinitrophenylhydrazine loaded sodium dodecyl sulfatecoated magnetite nanoparticles for adsorption of hg(II) ions from an aqueous solution. Ehemj. 3(4), 183–189 (2016)
- Yuan, L., et al.: Synthesis and characterization of mullite-ZrO2 porous fibrous ceramic for highly efficient oil-water separation. Ceram. Int. 47(16), 22709–22716 (2021)

- Ntholeng, N., et al.: Properties of Porous Mullite Filter Material fabricated from reaction sintered Mullite grains. J. Mater. Eng. Perform. 33(14), 7040–7053 (2024)
- Fouad, O.A., et al.: Fabrication and characterization of mullite nano-ceramic materials for use in carbon paste ion selective electrode to estimate carcinogenic cd (II) ion in real and human samples. Microchem. J. 190, 108623 (2023)
- Yang, J., et al.: Mullite ceramic foams with tunable pores from dual-phase sol nanoparticle-stabilized foams. J. Eur. Ceram. Soc. 42(4), 1703–1711 (2022)
- Luo, L., et al.: Facile synthesis of boehmite/PVA composite membrane with enhanced adsorption performance towards Cr(VI). J. Hazard. Mater. 318, 452–459 (2016)
- Tang, D., et al.: Design and application of Portable Centrifuge inspired by a Hand-Powered Spinning Top. Micromachines. 14 (2023). https://doi.org/10.3390/mi14101968
- Covaliu-Mierlä, C.I., Păunescu, O.: Iovu recent advances in membranes used for nanofiltration to remove Heavy metals from Wastewater: A review. Membranes. 13 (2023). https://doi.org/ 10.3390/membranes13070643
- Bastani, D., Esmaeili, N., Asadollahi, M.: Polymeric mixed matrix membranes containing zeolites as a filler for gas separation applications: A review. J. Ind. Eng. Chem. 19(2), 375–393 (2013)
- 19. UNDP: Human Development Report 2006. UNDP (United Nations Development Programme (2006)
- Judd, S.: The MBR Book: Principles and Applications of Membrane Bioreactors for Water and Wastewater Treatment. Elsevier Science (2010)
- Chatterjee, A., Basu, J.K., Jana, A.K.: Alumina-silica nanosorbent from plant fly ash and scrap aluminium foil in removing nickel through adsorption. Powder Technol. 354, 792–803 (2019)
- Barea, R., et al.: Thermal conductivity of highly porous mullite material. Acta Mater. 53(11), 3313–3318 (2005)
- She, J., Ohji, T.: Fabrication and characterization of highly porous mullite ceramics. Mater. Chem. Phys. 80(3), 610–614 (2003)
- Auger, M., Sarin, V.: The development of CVD mullite coatings for high temperature corrosive applications. Surf. Coat. Technol. 94, 46–52 (1997)
- Liu, Y.-F., et al.: Porous mullite ceramics from national clay produced by gelcasting. Ceram. Int. 27(1), 1–7 (2001)
- 26. Schneider, H., Komarneni, S.: Basic properties of mullite, in Mullite. Wiley Online Library. pp. 141–225. (2005)
- Fischer, R.X., Schneider, H.: Crystal chemistry of borates and borosilicates with mullite-type structures: A review. Eur. J. Mineral. 20(5), 917–933 (2008)
- 28. Osawa, C.C., Bertran, C.A.: Mullite formation from mixtures of alumina and silica sols: Mechanism and pH effect. J. Braz. Chem. Soc. **16**(2), 251–258 (2005)
- 29. Pani, S., et al.: Cost effective and minimal time synthesis of mullite from a mine waste by thermal plasma process. Adv. Mater. Lett. **6**(4), 318–323 (2015)
- Li, D.X., Thomson, W.J.: Mullite formation from nonstoichiometric diphasic precursors. J. Am. Ceram. Soc. 74(10), 2382–2387 (1991)
- Pask, J.A.: Importance of starting materials on reactions and phase equilibria in the Al2O3 SiO2 system. J. Eur. Ceram. Soc. 16(2), 101–108 (1996)
- 32. Cividanes, L.S., et al.: Review of mullite synthesis routes by solgel method. J. Solgel Sci. Technol. **55**(1), 111–125 (2010)
- Chen, T., et al.: Synthesis and characterization of poly-aluminum silicate sulphate (PASS) for ultra-low density fiberboard (ULDF). RSC Adv. 5(113), 93187–93193 (2015)
- 34. Leivo, J., et al.: Evolution of aluminosilicate structure and mullite crystallization from homogeneous nanoparticulate sol-gel



- precursor with organic additives. J. Eur. Ceram. Soc. **28**(9), 1749–1762 (2008)
- Anilkumar, G.M., et al.: Effect of precursor pH on the formation characteristics of sol-gel mullite. Mater. Lett. 33(3), 117–122 (1997)
- Chen, Z., et al.: Dense and crack-free mullite films obtained from a hybrid sol–gel/dip-coating approach. J. Mater. Res. 32(9), 1665– 1673 (2017)
- Zhang, Y., et al.: Mullite fibers prepared by Sol-Gel Method using Aluminum Chloride Aluminum Isopropoxide and Tetraethylorthosilicate. Mater. Manuf. Processes. 26(4), 649–653 (2011)
- 38. Ge, M., et al.: Ultrafine pure mullite powder prepared by sol-gel method. J. Non-cryst. Solids. **147–148**, 565–568 (1992)
- 39. Padmaja, P., et al.: Characterisation of stoichiometric sol–gel mullite by fourier transform infrared spectroscopy. Int. J. Inorg. Mater. **3**(7), 693–698 (2001)
- Tan, H.B., et al.: Preparation of mullite fibres by sol–gel processes using aluminium carboxylates and tetraethylorthosilicate. Mater. Sci. Technol. 27(2), 568–572 (2011)
- 41. de Oliveira, T.C., et al.: The kinetic of mullite crystallization: Effect of water content. J. Non-cryst. Solids. **356**(52), 2980–2985 (2010)
- Destaye, A.G., Lin, C.-K., Lee, C.-K.: Glutaraldehyde Vapor cross-linked Nanofibrous PVA mat with in situ formed silver nanoparticles. ACS Appl. Mater. Interfaces. 5(11), 4745–4752 (2013)
- Chen, Z., et al.: Pyrolysis behaviors and kinetic studies on Eucalyptus residues using thermogravimetric analysis. Energy. Conv. Manag. 105, 251–259 (2015)
- Wang, D.J., Kang, Y.F., Xu, B.P.: Preparation and Thermal decomposition of the Polyoxometalate complexes of Ciprofloxacin with HnXW12O40 (X=B, Si, P). Adv. Mater. Res. 335–336, 1075–1078 (2011)
- Jiang, W.H., et al.: Effect of gelation process on Preparation of Aluminum Titanate Ultrafine Powder by Hydrolytic Sol-Gel Method. Mater. Sci. Forum, 745–746: pp. 690–695. (2013)
- Olszewski, A., et al.: Effect of bio-polyol molecular weight on the structure and properties of polyurethane-polyisocyanurate (PUR-PIR) foams. Sci. Rep. 14(1), 812 (2024)
- 47. He, F., Petuskey, W.T.: Low temperature mullite crystallization in Al-and Si-alkoxide derived homogeneous gels. Mater. Lett. **63**(30), 2631–2634 (2009)
- 48. Wang, Z.F., et al.: Preparation and morphology of mullite whiskers by sol-gel method. in Key Engineering Materials. Trans Tech Publ. (2007)

- Yu, X., et al.: Network engineering of a BTESE membrane for improved gas performance via a novel pH-swing method. J. Membr. Sci. 511, 219–227 (2016)
- Agliullin, M.R., et al.: Sol-gel synthesis of mesoporous aluminosilicates with a narrow pore size distribution and catalytic activity thereof in the oligomerization of dec-1-ene. Microporous Mesoporous Mater. 230, 118–127 (2016)
- Gören, R., et al.: Colloidal stability–slip casting behavior relationship in slurry of mullite synthesized by the USP method. Ceram. Int. 38(1), 679–685 (2012)
- Jagannath, R., et al.: Studies on the formation of mullite from diphasic Al2O3-SiO2 gel by Fourier transform infrared spectroscopy. (2011)
- Liu, Y., et al.: Structural characterizations of aluminosilicates in two types of fly ash samples from Shanxi Province, North China. Minerals. 9(6), 358 (2019)
- Thommes, M., et al.: Physisorption of gases, with special reference to the evaluation of surface area and pore size distribution (IUPAC Technical Report). Pure Appl. Chem. 87(9–10), 1051–1069 (2015)
- Rouquerol, J., Llewellyn, P., Rouquerol, F.: Is the BET equation applicable to microporous adsorbents? in Characterization of Porous Solids VII - Proceedings of the 7th International Symposium on the Characterization of Porous Solids (COPS-VII), Aixen-Provence, France, 26–28 May 2005. pp. 49–56. (2007)
- Dumeignil, F., et al.: Modification of structural and acidic properties of sol–gel-prepared alumina powders by changing the hydrolysis ratio. Appl. Catal. A. 241(1), 319–329 (2003)
- 57. Anbazhagan, S., Thiruvengadam, V., Sukeri, A.: An Amberlite IRA-400 Cl-ion-exchange resin modified with Prosopis juliflora seeds as an efficient Pb2+adsorbent: Adsorption, kinetics, thermodynamics, and computational modeling studies by density functional theory. RSC Adv. 11(8), 4478–4488 (2021)

Publisher's Note Springer Nature remains neutral with regard to jurisdictional claims in published maps and institutional affiliations.

Springer Nature or its licensor (e.g. a society or other partner) holds exclusive rights to this article under a publishing agreement with the author(s) or other rightsholder(s); author self-archiving of the accepted manuscript version of this article is solely governed by the terms of such publishing agreement and applicable law.

